

This item is the archived peer-reviewed author-version of:

Mechanisms of selective nanocarbon synthesis inside carbon nanotubes

Reference:

Khalilov Umedjon, Neyts Erik.- Mechanisms of selective nanocarbon synthesis inside carbon nanotubes
Carbon - ISSN 0008-6223 - 171(2021), p. 72-78
Full text (Publisher's DOI): <https://doi.org/10.1016/J.CARBON.2020.08.060>
To cite this reference: <https://hdl.handle.net/10067/1724590151162165141>

Mechanisms of selective nanocarbon synthesis inside carbon nanotubes

Umedjon Khalilov* and Erik C. Neyts

PLASMANT research group, NANOLab Center of Excellence, University of Antwerp,

Universiteitsplein 1, 2610 Antwerp, BELGIUM

*Corresponding author. E-mail: umedjon.khalilov@uantwerpen.be (Umedjon Khalilov)

The possibility of confinement effects inside a carbon nanotube provides new application opportunities, e.g., growth of novel carbon nanostructures. However, the understanding the precise role of catalyst-feedstock in the nanostructure synthesis is still elusive. In our simulation-based study, we investigate the Ni-catalyzed growth mechanism of encapsulated carbon nanostructures, *viz.* double-wall carbon nanotube and graphene nanoribbon, from carbon and hydrocarbon growth precursors, respectively. Specifically, we find that the tube and ribbon growth is determined by a catalyst-vs-feedstock competition effect. We compare our results, i.e., growth mechanism and structure morphology with all available theoretical and experimental data. Our calculations show that all encapsulated nanostructures contain metal (catalyst) atoms and such structures are less stable than their pure counterparts. Therefore, we study the purification mechanism of these structures. In general, this study opens a possible route to the controllable synthesis of tubular and planar carbon nanostructures for today's nanotechnology.

1. Introduction

Carbon nanotubes (CNTs) [1] are considered as promising materials for various applications in today's nanotechnology due to their unique electronic, structural and other extraordinary properties [2]. In addition, the possibility of confinement effects in their inner cavity provides new application opportunities [3-6]. Indeed, experimental synthesis of carbon peapods (i.e., encapsulated C_{60} fullerenes inside CNT and denoted as $C_{60}@CNT$) [3] has initiated the extensive exploration of a new chemistry within the nanosized hollow container. In particular, coalescence of fullerenes in single-walled CNT (SWNT) [7] by heating or electronic irradiation in vacuum leads to form an inner tube inside the host tube [3, 4]. This method is an effective way of non-catalytic growth of double-walled CNT (DWNT), which has higher mechanical strength and better thermal and chemical stability than SWNT [8, 9]. In addition, narrow-diameter DWNTs are recognized as excellent confinement hosts to growth a new carbon allotrope – carbyne [10], which surpasses many other materials in mechanical properties, including carbon nanotubes, graphene and diamond [11].

Alternatively, the interaction of non-fullerene molecules inside an SWNT allows for the controlled design of various carbon nanostructures [4-6, 10, 12], including graphene nanoribbons (GNRs) [13, 14]. In particular, electronic and magnetic properties of GNRs can be modified by altering their geometry and dimensions [15-17]. Among various synthesis techniques, including unzipping of carbon nanotubes [18, 19] or cutting graphene sheets by plasma etching [20], a fusion of polycyclic aromatic hydrocarbons (PAH) in an SWNT provides the possibility to obtain encapsulated GNRs with a width ranging 1-2 nm [14, 16, 17], which is of great interest for various applications [21-24].

Besides their use as hydrocarbon growth precursors, metal-containing molecules are involved in catalyzing reactions in order to synthesize different carbon nanostructures, including tubes and ribbons, inside a SWNT [5, 6, 25-30]. In particular, metallofullerenes (i.e., fullerenes

containing metal atoms encapsulated in a SWNT denoted as $M@C_{60}@SWNT$) are used to enhance the fullerene-to-tube transformation inside the host tube and subsequent form DWNTs encapsulating metal nanowires [6, 31, 32]. Also, metallocenes [25] and metal acetylacetonates [6] have been investigated to catalyze the formation of inner tubes in a confined tubular environment. In particular, ferrocene ($FeCp_2$) and nickelocene ($NiCp_2$) molecules can act as catalysts and as a carbon source in the formation of a pure inner tube within a host tube [25, 33]. It was also reported that an inner carbon cap or a tube can be formed by only endohedral metal clusters under electron-beam irradiation [30]. In this feedstock-free growth process, several technologically important metals were separately encapsulated as a catalyst and SWNT-C atoms become a growth precursor after C-C bond breaking due to the interaction between the metal and the host-tube.

Despite tremendous experimental and theoretical studies, the precise role and effect of metal catalyst remains unclear in GNR growth encapsulated SWNT (i.e., $GNR@SWNT$). In particular, the growth mechanisms of $GNR@SWNT$ using metal-containing molecules or solely metal catalyst under e-beam irradiation have not been reported yet. Also, synthesis of encapsulated DWNTs or GNRs from simple carbon feedstocks, which are technological cheaper feedstock than fullerenes or metallocenes, is still elusive. Furthermore, the purification of metallocenes-assisted grown DWNT from metal particles [25, 33] is not explained in detail. In our present work, therefore, we theoretically investigate the dual role of feedstock and catalyst during the growth of encapsulated carbon nanostructures as well as the purification of the obtained structures. Particularly, we study the Ni-catalyzed nucleation and growth mechanisms of $SWNT@SWNT$, $carbyne@DWNT$ and $GNR@SWNT$ from carbon (C or C_2) and hydrocarbon (C_2H or C_2H_2) species, as well as the oxidation-based purification mechanism of these encapsulated carbon nanostructures (ECNs) from metal impurities, using reactive Molecular Dynamics (MD) simulations.

2. Simulation methods

2.1. ReaxFF. Simulations of the Ni-catalyzed growth of ECNs are performed using classical MD method. Bond formation and dissociation processes are described by the ReaxFF potential [34] with parameters developed by Zou et al. [35]. Previously, we demonstrated that this force field faithfully reproduces various key properties of the Ni/C/H/O system relevant for Ni-catalyzed CNT and carbyne growth from different carbon species [36-38].

2.2. Growth simulations. Periodic boundary conditions are applied to the simulation box with dimensions $3.0 \times 3.0 \times 2.2 \text{ nm}^3$. As a host tube, we use a (10,10) tube with a diameter of 1.36 nm. Mimicking an infinitely long SWNT, we position the tube along the z-axis. The z-length of the

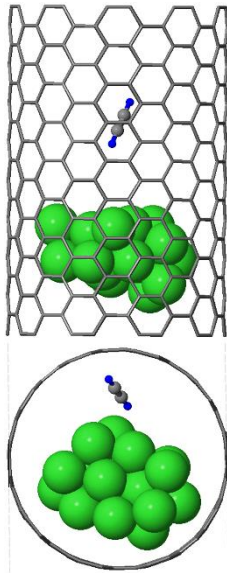


Figure 1. *Ni₁₈ nanocluster and C₂H₂ molecule inside (10,10) tube*

simulation box equals the tube length. Ni atoms are inserted in the host tube as catalyst [38]. The Ni_x@SWNT ($x = 5, 10, 13$ and 18) system (Fig. 1) is initially equilibrated at 1700 K applying the Berendsen thermostat and barostat (i.e., NpT ensemble) [39]. The endohedral atoms of Ni_x nanocluster are dynamic due to their weak Ni-C π connections to the concave wall-surface [27]. While the Ni bulk melting point ($\sim 1728 \text{ K}$) is higher than the growth temperature, the melting temperature considerable decreases by reducing the nanoparticle size, e.g., $T_M = 1200 \text{ K}$ for 4.3 nm diameter Ni nanoparticle [40]. Due to this size-dependent melting point depression or Gibbs-Tomson effect, endohedral Ni nanocluster can also be

fragmented during the nanostructure synthesis. Subsequently, we use the Bussi thermostat [41] to control the temperature during the NVT simulations. As a feedstock, a carbon atom/dimer (C or C₂) or an acetylene (C₂H, C₂H₂) molecule is randomly positioned inside a SWNT (Fig. 1). The initial velocity vector of the feedstock is randomized and its magnitude is set to the root-mean-square velocity corresponding to the growth temperature, i.e., 1700 K. The average time between two consecutive insertions is 0.1 ns. We assume that the tube length is long than

compared to the length of the any grown nanostructure and therefore, the gas-phase species are released from the system every 10^6 MD steps.

2.3. Purification simulations. During the oxidation of the ECNs@SWNT system, the concentration of gas-phase O atoms is kept constant at ~ 0.6 atoms \cdot nm $^{-3}$. In order to keep the constant gas density, a new O atom is included to the simulation box if one of gas-phase oxygen atoms connects to the tube.

3. Results and Discussion

3.1. Catalyzed growth mechanism of ECNs. Figure 2 demonstrates the intermediate steps of the catalyzed ECNs growth from the carbon (C or C₂) (Fig. 2a) and hydrocarbon feedstocks (C₂H or C₂H₂) inside a SWNT (Fig. 2b). Here, Ni₁₈ nanocluster is used as a catalyst. The concave surface of the SWNT interior is generally inert or unreactive and remains undamaged even when highly reactive species are encapsulated in the nanotube [5]. Therefore, an inserted carbon feedstock will rather connect to the encapsulated Ni atom/cluster. We find that the adsorption energy of the C-feedstock to the Ni decreases with increasing the N_H/N_C ratio, i.e., the adsorption energies are -3.68 eV for C₂ and -1.36 eV for C₂H₂ [38]. For both C₂ and C₂H₂ cases, Ni-C σ bonds form after two C-C π bonds are broken when these molecules chemisorb without fragmenting on the catalyst surface. During the dehydrogenation of C₂H₂, the molecule converts to ethynyl radical (C₂H) before it decomposes to a carbon (C₂) dimer. On the surface of the Ni cluster, diffusing H atoms recombine and desorb as H₂. We calculate the diffusion and the recombination barriers to be 0.51 eV and 1.22 eV, respectively [37]. In some cases, H₂ molecules can adsorb again onto the catalyst surface, as the adsorption barrier is low (0.24 eV). In all feedstock cases, remaining molecule fragments can diffuse on the catalyst surface before they connect to another adsorbed/dissociated carbon species. Such consecutive associations eventually lead to the formation of a carbon chain and consequent carbon ring (pentagon or

hexagon) on the catalyst surface (Figure 1a&b, 2 ns). Figure 2c shows that the chain-to-ring transformations in the C_x case is faster than the transformations in the C_xH_y case. In the growth process from C_x feedstock, a carbon cap appears after a formation of a graphene patch due to coalescence of carbon rings on the catalyst surface (Figure 2, 5 ns) [43]. The cap formation mechanism was also studied by Maruyama's group using both MD simulations and DFT calculations [44]. Besides, this cap formation phenomenon is similar to experimental findings, i.e., cap-nucleation occurring on an endohedral Ni nanocluster with about 1 nm-diameter inside

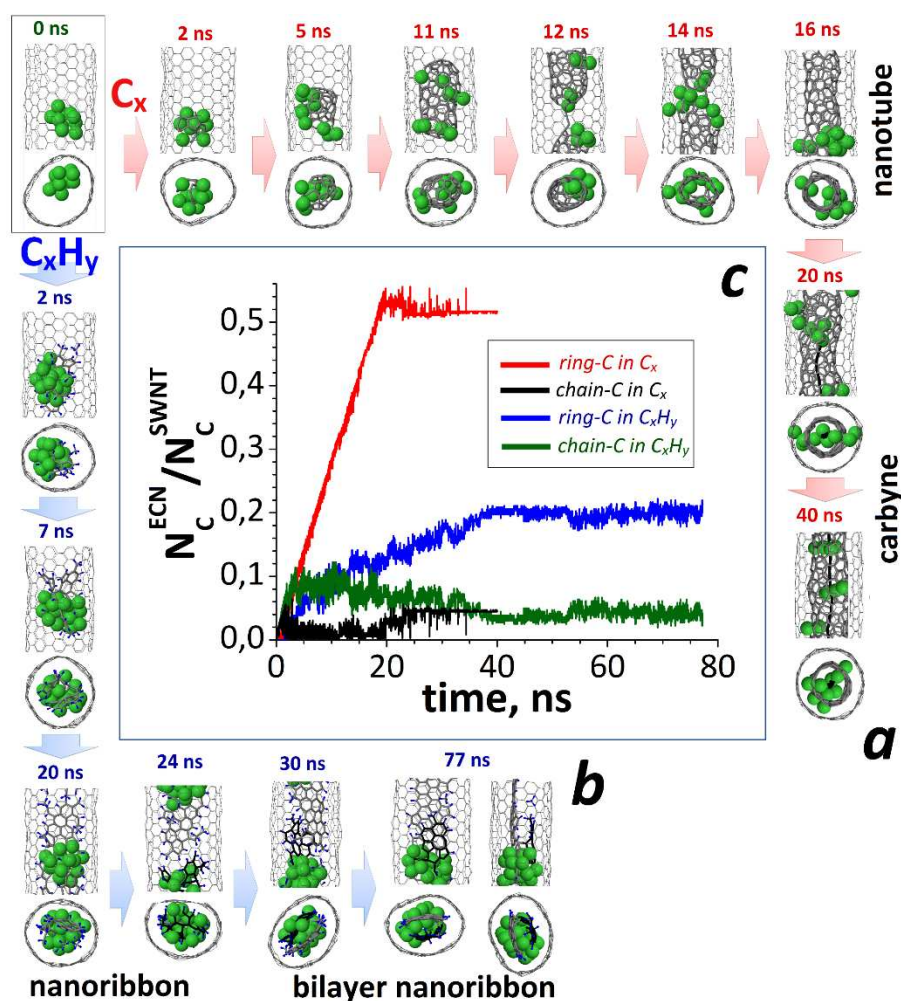


Figure 2 | Feedstock-based catalyzed growth: Catalyzed growth steps of different ECNs from C_x (a) and C_xH_y (b). Here, Ni, C and H atoms are in green, grey (or black) and blue colors, respectively. (c) The ratio between the number of ring or chain carbon atoms in ECN (N_C^{ECN}) and the number of carbon atoms in the host nanotube (N_C^{SWNT}) as a function of the growth time.

a SWNT [29, 30]. In these experiments, C atoms from the host-tube act as a growth precursor under 80 keV electron-beam irradiation (i.e., maximum kinetic energy transferred to transition metals is in the range of 1-4 eV [30]).

Subsequently, in our case, the cap gradually transforms to a fullerene with metal atoms (Figure 2a, 11 ns) such that the obtained structure resembles a metallofullerene peapod (fullerene containing metal atoms in SWNT) [4, 6, 27, 29, 45]. When separate metal clusters are present, several metallofullerenes can grow in the SWNT and they subsequently connect to each other through a carbon chain (Figure 2a, 12 ns) before they merge completely (Figure 2a, 14-16 ns). This phenomenon is an alternative to the fusion or dimerization of metallofullerenes encapsulated in SWNT [31, 46-48]. As a result, a metal-endohedral SWNT transforms to a metal-containing double-walled carbon nanotube (DWNT) [26, 44] (Figure 2a, 16 ns). We found that the average diameter of the obtained tube is 0.70 ± 0.15 nm and a difference between outer and inner diameters in our DWNT is about 0.33 ± 0.08 nm (see Figure S1 in the Supporting Information). Note that the difference with the experimental value of 0.36 ± 0.03 nm is within the error bar. Our value is also very close to the interlayer distances of DWNTs widely distributed in the range between 0.33 nm and 0.42 nm [49, 50]. Further experimental evidence reveals that the diameter difference shifts from 0.32 nm to 0.36 nm when the inner tube forms using ferrocene as the growth precursor instead of C₆₀ fullerene coalescence in the host tube [25]. It indicates that the diameter difference varies depending on feedstock and catalyst. Figure 1c shows that the concentration of carbon atoms in the inner wall (N_C^{ECN}) saturates when it reaches about half the number of carbon atoms in the host tube (N_C^{SWNT}). The N_C^{ECN}/N_C^{SWNT} ratio is about 0.51 (see Figure 2c) and it is fairly close to the ratio between the amounts of carbon atoms per 1D unit cell for inner (5,5) and outer (10,10) tubes. Also, in our results, the quality of the inner tube does not depend on the size of the nickel nanoparticle. In particular, we obtained DWNTs using a catalyst particle with different sizes, i.e., Ni₅, Ni₁₀ and

Ni₁₈, and we found that average contributions of pentagon, hexagon, heptagon and other rings are $22 \pm 1.4 \%$, $57 \pm 1.8 \%$, $18 \pm 1.0 \%$ and $3 \pm 1.1 \%$, respectively (see also Table S1 in the Supporting Information). Note in this respect that both the catalyst and the high growth temperature facilitate the appearance of pentagons and heptagons through Stone-Wales transformations [47, 51].

Continuous C_x supply gradually leads to the formation of a carbon chain or carbyne [10], confined inside the inner wall (Figure 2a, 20-40 ns). Figure 2c (black line) shows an increase in the number of chain C atoms until their amount saturates. This carbyne@DWNT structure (without a catalyst particle) has been experimentally observed and the results confirm that the (5,5) inner tube with a diameter of 0.71 nm inside (10,10) SWNT is an optimum among other tube diameters for carbyne growth [10]. Also, in our previous work, we demonstrated the catalyzed growth of encapsulated carbyne in (5,5)@(10,10) [38].

In the C_xH_y case, however, Fig. 2b demonstrates that different ECNs can grow. To understand the onset of differentiation in the structure morphology, all possible incipient carbon structures on Ni₁₃ cluster (demonstrated in Fig. 3) in the nucleation stage are analyzed as a function of their energy. Our previous NEB-MD calculations showed that the energy barriers for dimerization of C₂&C₂ and C₂H₂&C₂H₂ pairs (see structures 2 and 3 in Fig. 3) are 0.1 eV and 0.3 eV, respectively [38]. This strongly indicates that the (nickel) catalyst facilitates the formation of C-C connections, while hydrogen delays or prevents such connections. Consequently, such catalyst-hydrogen competition determines the rate of chain-ring-network formations. After a chain-ring transformation (see structures 4-6 in Fig. 3), hexagon carbon rings are sequentially formed on the catalyst nanocluster for both feedstock cases. During the ring formation, the formed network partially loses their H atoms, i.e., they desorb by the Langmuir–Hinshelwood (LH) recombinative desorption (after a recombination with another adsorbed H, or Hads&Hads) mechanism. Prior to appearance of fourth hexagon, all network

structures are planar for both feedstock cases (see structures 6-9 in Fig. 3), although they are in a free-standing position in the C_2H_2 case. The stability of such free-standing networks can be explained by the H-termination of the dangling bonds [36, 42].

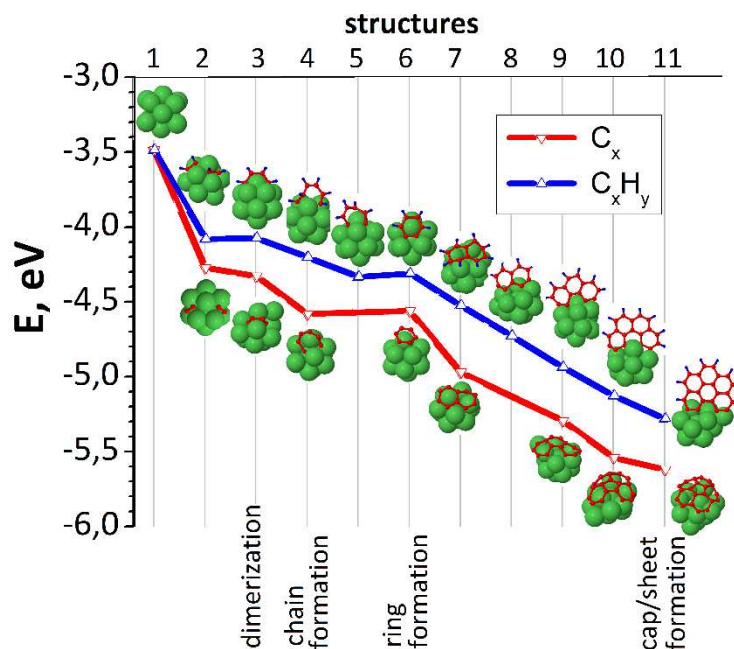


Figure 3 | *Energies of incipient structures in dimerization, chain, ring and cap/sheet formation steps of the nucleation stage of tube and graphene growth using C_2 and C_2H_2 feedstocks, respectively.*

When the fourth hexagon is formed in the C_2 case, an initial pentagon appears due to the connection of C atoms in the first and fourth hexagons (see structure 10 in Fig. 3). The Ni catalyst facilitates this C-C bond formation. On the other hand, in the C_2H_2 case, this connection does not appear in the H-terminated free-standing carbon network. Consequently, a carbon cap and a graphene sheet eventually appear in the cases of C_2 and C_2H_2 , respectively (see structure 11 in Fig. 3).

In the C_xH_y case, the appeared H-terminated and freestanding graphene patch/sheet [36] eventually transforms to a graphene nanoribbon (GNR) (Figure 2b, 5-16 ns). Subsequently, the graphene nanoribbon gradually grows inside the host tube, which is denoted as GNR@SWNT [6] (Figure 2b, 20 ns). We found that an average width of the encapsulated GNR is about 0.7

nm and the distance between the graphene edge and the host tube-wall is about 0.35 nm (see Figure S2 in the Supporting Information).

The GNR width in our simulations matches experimentally obtained GNRs terminated by hydrogen (H-GNR) or sulphur atoms (S-GNR) inside a SWNT with diameter of about 1.4 nm [52, 53]. Consistent with experimental evidences, we find that an optimal SWCNT diameter and a width of the formed GNR depend on the size of the inserted polycyclic aromatic hydrocarbon molecule [52]. The optimum range of internal diameters of SWCNT were reported to be between 1 - 2 nm and stable GNRs do not form outside of this range [53, 54]. In particular, the GNR structure becomes helical inside SWCNTs with a diameter larger than 1.5 nm [54] and the twisted nanoribbons subsequently converts to a nanotube [32]. In accordance with the narrow-diameter condition [53, 54], we obtain a non-helical H-GNR inside a (10,10) nanotube containing metal atoms [55] as a result of synergistic effect of metal catalyst and hydrocarbon molecule. While some pentagon rings are present in the grown GNR, their structure is similar to the structure of experimental grown GNRs obtained by the dimerization and oligomerization of coronene molecules [52].

Consecutive C_xH_y supply can germinate another H-GNR as well (Figure 2*b*, 24-30 ns). When a H-GNR meets a second H-GNR, they do not coalesce due to their H-terminated edges, and consequently a bilayer GNR (H-BGNR) grows inside the SWCNT (Figure 2*b*, 77 ns). This suggests that tuning the H content (by selecting the right hydrocarbon feedstock) and host-tube diameter allows to control the width and the layer quantity of the grown GNRs. At higher temperatures, BGNR can lose their edge H atoms to some extent and the structure can partially transform to an SWNT. This phenomenon can be an alternative to the transformation of twisted GNRs into SWNTs [6, 32]. Besides temperature effect, understanding the precise role of other growth parameters such as tube chirality and diameter is also important in the structure control. However, in this work, we mainly focus on the catalyst-feedstock effect.

3.2. Relative stability of the obtained ECNs. To evaluate the stability of metal-containing ECNs, we have chosen 10 different ideal structures, *i.e.*, SWNT@SWNT ($C_{540}H_{60}$), carbyne@DWNT ($C_{557}H_{62}$), GNR@SWNT ($C_{432}H_{50}$), H-GNR@SWNT ($C_{432}H_{66}$) and H-BGNR@SWNT ($C_{504}H_{92}$) with and without metal atoms, as shown in Figure 4. Here, each metal-containing ECN encloses 10 Ni atoms. In order to correctly evaluate the cohesive energy and relative stability, the total energy of a structure is minimized. During the minimization, a periodicity is not applied, *vis.*, dangling bonds of the structure are terminated by H atoms. The cohesive energy per atom indicates that the SWNT@SWNT is energetically the most favorable structure. In addition, the cohesive energy of the structures without metal atoms is lower than the energy of their metal-containing counterparts (open red and green squares in Figure 4).

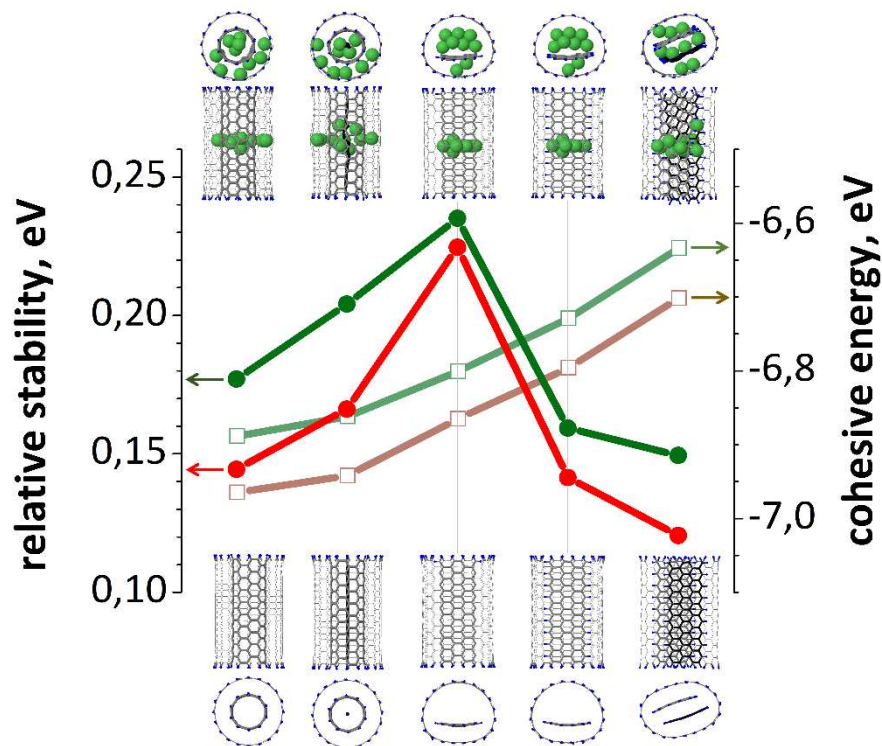


Figure 4 | Structure stability: Relative stabilities (solid circles) and cohesive energies per atom (open squares) for ECNs. Corresponding lines are indicated by arrows. Here, values related to bare and metal-containing structures are highlighted by red (or light braun) and green (or light green) colors, respectively.

However, nanostructures consist of different chemical compounds and hence the cohesive energy is not a suitable parameter to compare the stability of those systems. Based on the previous analysis for the relative thermodynamic stability of endohedral Si nanotubes [56] and bare/passivated GNRs [57], we estimate the relative stability by a molar (per atom) Gibbs free energy of formation δG for ECNs as follows:

$$\delta G = E - x_C\mu_C - x_H\mu_H - x_{Ni}\mu_M \quad (1)$$

where E is the cohesive energy per atom of the ECN. The molar fractions of carbon, hydrogen and metal (nickel) atoms in the structure are denoted by x_C , x_H and x_M , respectively, while μ_C , μ_H and μ_M denote the chemical potentials of the constituents. In our case, μ_C and μ_M are chosen as the cohesive energy per atom of a single graphene sheet (-7.64 eV) and Ni bulk (-4.45 eV), respectively. The μ_H equals the binding energy per atom of the H₂ molecule (-2.36 eV).

The δG calculations show that H-GNR@SWNT and H-BGNR are more stable than SWNT@SWNT and carbyne@DWNT, as shown in Figure 4. It can also be seen that GNR@SWNT is the least stable structure among the ECNs. This conclusion is confirmed by DFT calculations as well, i.e., GNRs that are terminated with heteroatoms (including H atoms) are more stable than SWNT, while bare GNRs are thermodynamically less stable than SWNTs due to the dangling bonds along its edges [41, 57]. Furthermore, the trend is identical for structures with metal atoms (solid green circles in Figure 4). However, metal-containing ECNs are less stable than their bare counterparts for all cases and therefore a purification step would increase the stability of ECNs.

3.3. Purification mechanism of ECNs. As an example, Figure 5a demonstrates purification steps of H-GNR@SWNT from Ni atoms due to oxidation. During the oxidation process, a defect hole is first created when an impinging O atom detaches from the host-tube C atom (Figure 5a, 1.5 ns). Accordingly, the number of hexagon rings in the SWNT decreases (Figure

5b, dark blue). Evolution of a number of hexagons and their fractions over all types of rings before the hole formation on the tube surface is schematically demonstrated in Figure S3 in the Supporting Information. A nickel atom may then exit through the hole and interact with gas-phase O atom(s) (Figure 5a, 4.5 ns). In some cases, two or more holes are simultaneously created on the host tube and consequently they are plugged by Ni atoms (see Figure S4 in the Supporting Information). Due to Ni-O bond formation, Ni-C bonds break and endohedral Ni atoms withdraw one-by-one from the SWNT to gradually form an NiO cluster on the tube sidewall (Figure 5a, 5.0 ns) before it completely leaves the tube (Figure 5a, 5.5 ns). As a result, the Ni content in the system decreases two times (Figure 5b, 5.5 ns, red line). Also, stepwise decreases for the ratio $N_{\text{Ni}}/N_{\text{C}}$ (Figure 5b, 5.5-16 ns, red line) during the oxidation indicate that

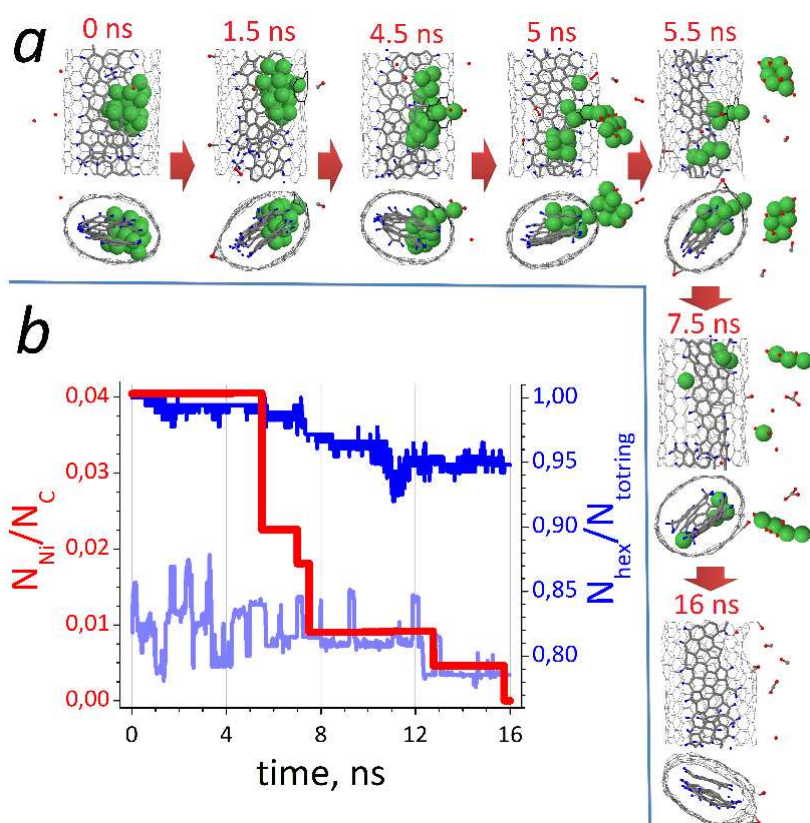


Figure 5 | Purification steps: (a) Purification steps of H-GNR@SWNT from nickel atoms. (b) Evolution of the ratio between nickel and carbon atoms (red color) as well as the fraction of hexagonal rings in the tube (dark blue) and ribbon (light blue) during the purification process.

amount of oxidized nickel atoms reduces stepwise (Figure 5a, 7.5 ns). Eventually, the SWNT releases all metal atoms and thus only the H-GNR remains in the host tube (Figure 5a, 16 ns). While the tube loses about 5% of its hexagon rings during the formation of defect hole(s) (Figure 5b, dark blue lines), the quality of encapsulated H-GNR seems to be retained (Figure 5b, light blue lines). Although the number of hexagon carbon rings in H-GNR fluctuates around 7% which corresponds to addition/removal of one hexagon, the network retains nearly all rings due to H-termination of its dangling bonds. On the other hand, the encapsulated carbyne structure in SWNT is completely etched during the purification (see Figure S5 in the Supporting Information). The results indicate that at least two endohedral Ni atoms are required to stabilize and retain the carbyne.

Alternatively, oxygen-assisted purification of metal-containing SWNT@SWNT has been experimentally reported [25, 33]. In particular, the authors grew an inner tube via filling SWCNTs by NiCp₂ [33] or FeCp₂ molecules [25]. Subsequently, Ni or Fe atoms precipitate onto the DWCNT surface forming their oxide on the tube surface by subsequent oxidation. However, the purification onset is not properly explained. To understand the purification mechanism, we schematically demonstrate the process (Figure 6), dividing it into two stages: formation of a SWNT hole and subsequent blocking the hole by a Ni atom (stage I), and detaching of the plug (Ni) atom(s) one-by-one (stage II).

In Stage I, when an incoming single oxygen atom adsorbs onto the SWNT by connecting to two C atoms, the sp² character of both carbon atoms converts to quasi sp³. This increases the local curvature (or pyramidalization angle [58]) of the nanotube and increases the reactivity of this site. As a result, endohedral Ni atoms preferably move towards this site [27]. The oxygen connection to the tube and subsequent nickel linkage to this site lower the system potential energy (per atom) to -0.65 eV and -1.32 eV, respectively. Due to both oxygen and nickel connections, the C-C bond in the defective site is eventually broken and one of C atoms can be

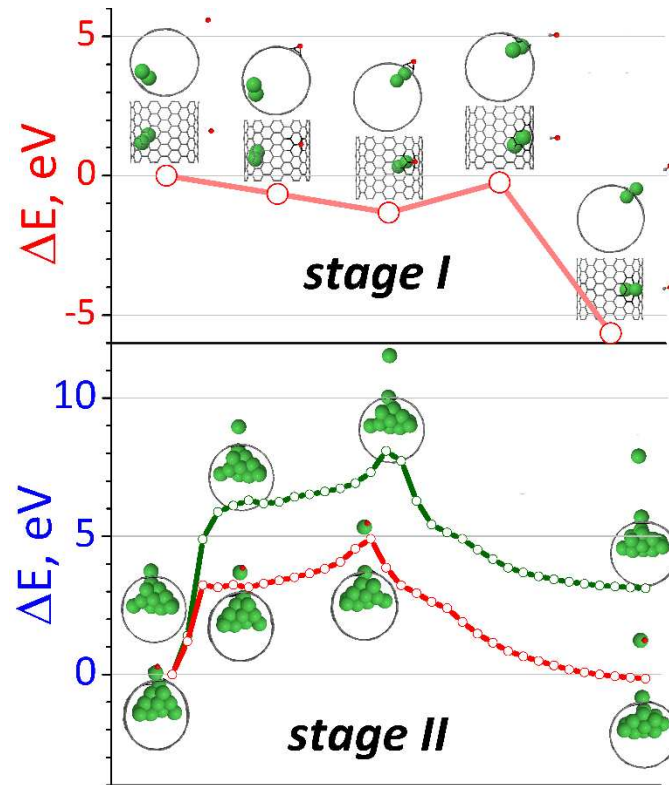


Figure 6 | Purification stages: Two stages of the purification process. Here, ΔE is the energy difference between the structure and its original (first) structure.

detached by the adsorbed oxygen atom. This C-C dissociation and C-O detachment due to C-Ni bond formation is a similar to the experimental evidence of C ejection during e -beam irradiation of Ni@SWNT [30]. Subsequently, as shown in Figure 6, stage I, the SWNT with a defect hole connects to Ni atom, which is energetically more stable (-0.24 eV) than the pristine SWNT, although the creation of the hole requires to overcome an energy barrier of about 1.10 eV. Namely, the Ni-C π bond converts to a Ni-C σ bond due to C atoms with “dangling” bonds at the edge of the hole. Thus, the Ni atom shifts from the concave inner to the convex outer surface [58] and it thus completely blocks the SWNT hole. This structure is the most favorable of structures in this stage, i.e, the system energy decreases by up to -5.64 eV.

Stage II consists of two steps: (1) detaching (extraction) of a blocking or a plug (Ni) atom and (2) a hole blocking by other endohedral Ni atom (Figure 6, stage II). Our NEB-MD calculations

show that the removal of the plug atom requires overcoming an energy barrier of 6.3 eV. This energy barrier decreases by a factor of 2 when plug Ni contains O atom(s). Obviously, the oxidation process significantly catalyzes the extraction of plug (Ni) atoms. After the removal, another endohedral Ni blocks the tube hole (with an energy barrier of about 1.7 eV) and it thus hinders gas-phase species to enter the host-tube. Such plug effect was also experimentally observed, i.e., trapped Gd atoms at the hole of a single-walled nanohorn greatly reduce permeation of molecules, including fullerenes [59]. Our results show that extraction of plug atom is endergonic (3.12 eV), while it becomes exergonic (-0.15 eV) when the plug atom is oxidized. This indicates that the oxidation is an options for purifying ECNs. Further, these two steps cycle until the tube releases all endohedral metal atoms.

4. Conclusion

We theoretically study Ni-catalyzed growth mechanism of encapsulated cap/fullerene inside SWCNTs, double-walled carbon nanotubes (DWCNTs) and enclosed carbyne in DWCNTs from C_x (C or C_2) feedstocks, as well as single or bilayer graphene nanoribbons (GNRs) from C_2H_2 molecule. We find that such growth behavior is due to catalyst-vs-hydrogen effects: the Ni catalyst facilitates the chain-ring-cap transformations, while H atoms delay or prevent such transformations. As a result, either a carbon cap in the C_x case or a freestanding graphene patch in the C_xH_y case can be grown as initial structures. Prior to DWCNT and carbyne growth, the formation mechanisms of intermediate structures, including carbon cap and metallofullerene peapod are also discussed in comparison with experimental evidences as well as other simulation/calculations results. Also, the morphology of the obtained tubular, planar and linear structures is analyzed and compared to experimental results.

Obviously, all encapsulated structures contain metal (Ni) atoms. We find that the stability of the Ni-containing structures is less than the stability of their pure counterparts. Consequently,

it is beneficial to purify these structures from Ni atoms, e.g. using oxidation. We explain the purification mechanism dividing it into two steps: (i) defect hole creation and metal plugging, and (ii) consecutively detachment of plugged metal atoms. The results indicate that thoroughly understanding the purification nature and thus its manipulation leads to structure control.

Overall, the results indicate that structure control highly depends on the choice of catalyst and feedstock. A comprehensive understanding of the synthesis mechanisms motivates controlled formation of nanomaterials with controllable dimensions.

Acknowledgment

The authors gratefully acknowledge the financial support from the Fund of Scientific Research Flanders (FWO), Belgium, Grant number 12M1318N. The work was carried out in part using the Turing HPC infrastructure of the CalcUA core facility of the Universiteit Antwerpen (UA), a division of the Flemish Supercomputer Centre VSC, funded by the Hercules Foundation, the Flemish Government (department EWI) and the UA, Belgium.

References

1. S. Iijima, Helical microtubules of graphitic carbon. *Nature* 354 (1991) 56-58.
2. M. F. L. De Volder, S. H. Tawfick, R. H. Baughman, A. J. Hart, Carbon Nanotubes: Present and Future Commercial Applications. *Science* 339 (2013) 535-539.
3. B. W. Smith, M. Monthieux, D. E. Luzzi, Encapsulated C₆₀ in carbon nanotubes. *Nature* 1998, 396, 323-324.
4. A. N. Khlobystov, D. A. Britz and G. A. D. Briggs, Molecules in Carbon Nanotubes. *Acc. Chem. Res.* 2005, 38, 901-909.

5. X. Pan and X. Bao, The Effect of Confinement inside Carbon Nanotubes on Catalysis. *Acc. Chem. Res.* 2011, 44, 553-562.
6. H. Shinohara, Peapods: Exploring the inner space of carbon nanotubes. *Jpn. J. Appl. Phys.* 57, 020101 (2018)
7. S. Iijima & T. Ichihashi, Single-shell carbon nanotubes of 1-nm diameter. *Nature* 363 (1993) 603-605.
8. T. P. R. Pfeiffer, Y. A. Kim, H. Kuzmany, Double-Wall Carbon Nanotubes, ed. G. D. A. Jorio, M. S. Dresselhaus, Springer-Verlag, 2008.
9. C. Shen, A. H. Brozena and Y. H. Wang, Double-walled carbon nanotubes: Challenges and opportunities. *Nanoscale* 2011, 3, 503-518.
10. L. Shi, P. Rohringer, K. Suenaga, Y. Niimi, J. Kotakoski, J. C. Meyer *et al.* Confined linear carbon chains as a route to bulk carbyne. *Nature Mater.* **15**, 634–640 (2016).
11. M. Liu, V. I. Artyukhov, H. Lee, F. Xu, B. I. Yakobson, Carbyne from first principles: chain of C atoms, a nanorod or a nanorope? *ACS Nano* 7 (2013) 10075-10082.
12. J. Zhang, *et al.*, Synthesis and transformation of linear adamantane assemblies inside carbon nanotubes. *ACS Nano* 6 (2012) 8674-8683.
13. Geim, A. K. & Novoselov, K. S. The rise of graphene. *Nature Mater.* 6,183–191(2007).
14. X. Li, X. Wang, L. Zhang, S. Lee, H. Dai, Chemically derived, ultrasoft graphene nanoribbon semiconductors. *Science* 319, 1229–1232 (2008).
15. Nakada, K., Fujita, M., Dresselhaus, G. & Dresselhaus, M. S. Edge state in graphene ribbons: nanometer size effect and edge shape dependence. *Phys. Rev. B* 54,17954–17961 (1996).
16. Son, Y.-W., Cohen, M. L. & Louie, S. G. Energy gaps in graphene nanoribbons. *Phys. Rev. Lett.* 97, 216803 (2006).

17. Han, M. Y., Oezylmaz, B., Zhang, Y. & Kim, P. Energy band-gap engineering of graphene nanoribbons. *Phys. Rev. Lett.* 98, 206805 (2007).
18. D. V. Kosynkin, A. L. Higginbotham, A. Sinitskii, J. R. Lomeda, A. Dimiev, B. K. Price & J. M. Tour Longitudinal unzipping of carbon nanotubes to form graphene nanoribbons. *Nature* 2009, 458, 872-877.
19. L. Jiao, L. Zhang, X. Wang, G. Diankov, H. Dai, Narrow graphene nanoribbons from carbon nanotubes. *Nature*. **458** (2009) 877–80.
20. Ci, L. J. *et al.* Controlled nanocutting of graphene. *Nano Res.* 1, 116–122 (2008).
21. Chen, Z., Lin, Y.-M., Rooks, M. J. & Avouris, P. Graphene nano-ribbon electronics. *Physica E* 40, 228–232 (2007).
22. M. A. Raifee, W. Lu, A. V. Thomas, A. Zandiatashbar, J. Rafiee, J. M. Tour, N. Koratkar, Graphene Nanoribbon Composites. *ACS Nano* 4 (2010) 7415–7420.
23. G. Lalwani, A. M. Henslee, B. Farshid, L. Lin, F. K. Kasper, Y.-X. Qin, A. G. Mikos, B. Sitharaman, Two-Dimensional Nanostructure-Reinforced Biodegradable Polymeric Nanocomposites for Bone Tissue Engineering. *Biomacromolecules* 2013, 14, 900–909.
24. G. Lalwani, X. Cai, L. Nie, L. V. Wang, B. Sitharaman, Graphene-based contrast agents for photoacoustic and thermoacoustic tomography. *Photoacoustics* 1 (2013) 62–67.
25. H. Shiozawa, T. Pichler, A. Grüneis, R. Pfeiffer, H. Kuzmany, Z. Liu, K. Suenaga, and H. Kataura, A Catalytic Reaction Inside a Single-Walled Carbon Nanotube. *Adv. Mater.* 2008, 20, 1443–1449.
26. R. Kitaura, R. Nakanishi, T. Saito, H. Yoshikawa, K. Awaga, and H. Shinohara, High-Yield Synthesis of Ultrathin Metal Nanowires in Carbon Nanotubes. *Angew. Chem. Int. Ed.* 2009, 48, 8298 –8302.

27. J. H. Warner, Y. Ito, M. H. Rummeli, T. Gemming, B. Buchner, H. Shinohara, and G. A. D. Briggs, One-Dimensional Confined Motion of Single Metal Atoms inside Double-Walled Carbon Nanotubes. *Phys Rev. Lett.* 102 (2009) 195504.
28. P. Serp and E. Castillejos, Catalysis in Carbon Nanotubes. *Chem. Cat. Chem.* 2010, 2, 41-47.
29. A. S. Sinitsa, T. W. Chamberlain, T. Zoberbier, I. V. Lebedeva, A. M. Popov, A. A. Knizhnik *et al.* Formation of Nickel Clusters Wrapped in Carbon Cages: Toward New Endohedral Metallofullerene Synthesis. *Nano Lett.* 2017, 17, 1082–1089.
30. K. Cao, T. Zoberbier, J. Biskupek, A. Botos, R. L. McSweeney, A. Kurtoglu, Comparison of atomic scale dynamics for the middle and late transition metal nanocatalysts. *Nat. Commun.* 9 (2018) 3382.
31. K. Hirahara, K. Suenaga, S. Bandow, H. Kato, T. Okazaki, H. Shinohara and S. Iijima, One-Dimensional Metallofullerene Crystal Generated Inside Single-Walled Carbon Nanotubes. *Phys. Rev. Lett.* 85, 5384 (2000).
32. H. E. Lim, Y. Miyata, R. Kitaura, Y. Nishimura, Y. Nishimoto, S. Irle, J. H. Warner, H. Kataura and H. Shinohara, Growth of carbon nanotubes via twisted graphene nanoribbons. *Nat. Commun.* 4, 2548 (2013).
33. M. V. Kharlamova, M. Sauer, T. Saito, Y. Sato, K. Suenaga, T. Pichler and H. Shiozawa, Doping of single-walled carbon nanotubes controlled via chemical transformation of encapsulated nickelocene. *Nanoscale* 2015, 7, 1383.
34. A. C. T. van Duin, S. Dasgupta, F. Lorant, W. A. Goddard III, ReaxFF: a reactive force field for hydrocarbons. *J. Phys. Chem. A* 105 (2001) 9396e9409.
35. C. Zou, Y.K. Shin, A.C.T. van Duin, H. Fang, Z.-K. Liu, Molecular dynamics simulations of the effects of vacancies on nickel self-diffusion, oxygen diffusion and oxidation initiation in nickel, using the ReaxFF reactive force field. *Acta Mater.* 83 (2015) 102e112.

36. U. Khalilov, A. Bogaerts and E. C. Neyts, Atomic scale simulation of carbon nanotube nucleation from hydrocarbon precursors. *Nat. Commun.*, 2015, 6, 10306.
37. U. Khalilov, C. Vets, E. C. Neyts, Molecular evidence for feedstock-dependent nucleation mechanisms of CNTs. *Nanoscale Horizons* 4, 674-682 (2019).
38. U. Khalilov, C. Vets, E. C. Neyts, Catalyzed growth of encapsulated carbyne. *Carbon* 153, 1-5 (2019).
39. H. J. C. Berendsen, J.P.M. Postma, W.F. van Gunsteren, A. Di Nola, J.R. Haak Molecular dynamics with coupling to an external bath. *J. Chem. Phys.* 81 (1984) 3684e3690.
40. A. van Teijlingen, S. A. Davis and S. R. Hall, Size-dependent melting point depression of nickelnanoparticles. *Nanoscale Adv.* 2020, 2, 2347-2351.
41. G. Bussi, D. Donadio, M. Parrinello, Canonical sampling through velocity rescaling. *J. Chem. Phys.* 126 (2007) 014101.
42. A. Chuvilin, E. Bichoutskaia, M. C. Gimenez-Lopez, T.W. Chamberlain, G. A. Rance, N. Kuganathan *et al.* Self-assembly of a sulphur-terminated graphene nanoribbon within a single-walled carbon nanotube. *Nature Mater* **10**, 687–692 (2011).
43. E. C. Neyts, Y. Shibuta, A. C. T. van Duin, A. Bogaerts, Catalyzed Growth of Carbon Nanotube with Definable Chirality by Hybrid Molecular Dynamics– Force Biased Monte Carlo Simulations. *ACS Nano* 4 (2010) 6665-6672.
44. Y. Izu, J. Shiomi, Y. Takagi, S. Okada, and S. Maruyama, Growth Mechanism of Single-Walled Carbon Nanotube from Catalytic Reaction Inside Carbon Nanotube Template. *ACS Nano* 2010, 4, 4769-4775.
45. Y. Yamaguchi, S. Maruyama, A Molecular Dynamics Study on the Formation of Metallofullerene. *Euro. Phys. J. D* 1999, 9, 385–388.

46. M. Koshino, Y. Niimi, E. Nakamura, H. Kataura, T. Okazaki, K. Suenaga and S. Iijima, Analysis of the reactivity and selectivity of fullerene dimerization reactions at the atomic level. *Nat. Chem.* 2010, 2, 117-124.
47. Z. Xu, H. Li, K. Fujisawa, Y. A. Kim, M. Endo and F. Ding, Multiple intra-tube junctions in the inner tube of peapod-derived double walled carbon nanotubes: theoretical study and experimental evidence. *Nanoscale*, 2012, 4, 130.
48. Y. Shibuta, S. Maruyama, Molecular Dynamics of Generation Process of Double-Walled Carbon Nanotubes from Peapods. *Heat Transfer Asian Res.* 2006, 35, 254–264.
49. Y. J. Li, K. L. Wang, J. Q. Wei, Z. Y. Gu, Z. C. Wang, J. B. Luo and D. H. Wu, Tensile properties of long aligned double-walled carbon nanotube strands. *Carbon* 2005, 43, 31-35.
50. K. Hirahara, M. Kociak, S. Bandow, T. Nakahira, K. Itoh, Y. Saito and S. Iijima, Chirality correlation in double-wall carbon nanotubes as studied by electron diffraction. *Phys. Rev. B* 2006, 73, 195420.
51. C. P. Ewels, M. I. Heggie, P. R. Briddon, Adatoms and nanoengineering of carbon. *Chemical Physics Letters* 351 (2002) 178-182.
52. A. V. Talyzin, I. V. Anoshkin, A. V. Krashennnikov, R. M. Nieminen, A. G. Nasibulin, H. Jiang and E. I. Kauppinen, Synthesis of Graphene Nanoribbons Encapsulated in Single-Walled Carbon Nanotubes. *Nano Lett.* 2011, 11, 4352–4356.
53. T. W. Chamberlain, J. Biskupek, G. A. Rance, A. Chuvilin, T. J. Alexander, E. Bichoutskaia, U. Kaiser and A. N. Khlobystov, Size, Structure, and Helical Twist of Graphene Nanoribbons Controlled by Confinement in Carbon Nanotubes. *ACS Nano* 6, 3943 (2012).
54. Y. Jiang, H. Li, Y. Li, H. Yu, K. M. Liew, Y. He, and X. Liu, Helical Encapsulation of Graphene Nanoribbon into Carbon Nanotube. *ACS Nano* 5, 2126 (2011).

55. Y. Wang, C. Cao and H.-P. Cheng, Metal-terminated graphene nanoribbons. *Phys. Rev. B* 2010, 82, 205429.
56. T. Dumitrică, M. Hua and B. I. Yakobson, Endohedral silicon nanotubes as thinnest silicide wires. *Phys. Rev. B* **70**, 241303 (2004).
57. V. Barone, O. Hod and G. E. Scuseria, Electronic Structure and Stability of Semiconducting Graphene Nanoribbons. *Nano Lett.*, 6, 2748-2754 (2006).
58. S. Niyogi, M. A. Hamon, H. Hu, B. Zhao, P. Bhowmik, R. Sen, et al. Chemistry of Single-Walled Carbon Nanotubes. *Acc. Chem. Res.* 2002, 35, 1105-1113.
59. A. Hashimoto, H. Yorimitsu, K. Ajima, K. Suenaga, H. Isobe, J. Miyawaki *et al.* Selective deposition of a gadolinium(III) cluster in a hole opening of single-wall carbon nanohorn. *PNAS* 2004, 101, 8527-8530.